# Dynamics and phase diagram of the $\nu=0$ quantum Hall state in bilayer graphene

E. V. Gorbar and V. P. Gusynin
*Bogolyubov Institute for Theoretical Physics, 03680 Kiev, Ukraine*

V. A. Miransky*
*Department of Applied Mathematics, University of Western Ontario, London, Ontario, Canada N6A 5B7*
(Received 30 March 2010; published 26 April 2010)

Utilizing the Baym-Kadanoff formalism with the polarization function calculated in the random phase approximation, the dynamics of the $\nu=0$ quantum Hall state in bilayer graphene is analyzed. Two phases with nonzero energy gap, the ferromagnetic and layer asymmetric ones, are found. The phase diagram in the plane $(\tilde{\Delta}_0, B)$, where $\tilde{\Delta}_0$ is a top-bottom gates voltage imbalance, is described. It is shown that the energy gaps in these phases scale linearly, $\Delta E \sim 10B$ [T]K, with magnetic field. The comparison of these results with recent experiments in bilayer graphene is presented.

DOI: 10.1103/PhysRevB.81.155451 PACS number(s): 73.43.Cd, 71.70.Di, 81.05.U−

## I. INTRODUCTION

The properties of bilayer graphene,[1–5] consisting of two closely coupled graphene layers, have attracted great interest. The possibility of inducing and controlling the energy gap by gates voltage makes bilayer graphene one of the most active research areas with very promising applications in electronic devices. Recent experiments in bilayer graphene[6,7] showed the generation of energy gaps in a magnetic field with complete lifting of the eightfold degeneracy in the zero-energy Landau level, which leads to new quantum Hall states with filling factors $\nu=0, \pm 1, \pm 2, \pm 3$. Besides that, in suspended bilayer graphene, Ref. 6 reports the observation of an extremely large magnetoresistance in the $\nu=0$ state due to the energy gap $\Delta E$, which scales linearly with a magnetic field $B$, $\Delta E \sim 3.5-10.5B$ [T]K, for $B \lesssim 10$ T. This linear scaling is hard to explain by the standard mechanisms[8,9] of gap generation used in a monolayer graphene, which lead to large gaps on the order of the Coulomb energy $e^2/l \sim B^{1/2}$, $l=(\hbar c/eB)^{1/2}$ is the magnetic length.

The theory of the quantum Hall effect (QHE) in bilayer graphene has been studied in Refs. 10–14. In particular, the gap equation for the quasiparticle propagator including the polarization screening effects has been recently studied in Refs. 13 and 14. While a polarization function with no magnetic field was used in Ref. 13, the polarization function with a magnetic field was utilized in Ref. 14.

In this paper, we study the dynamics of clean bilayer graphene in a magnetic field, with the emphasis on the $\nu=0$ state in the QHE (a brief description of a part of the results of this study was presented in Ref. 14). It will be shown that, as in the case of monolayer graphene,[15] the dynamics in the QHE in bilayer graphene is described by the *coexisting* quantum Hall ferromagnetism[8] (QHF) and magnetic catalysis[9] (MC) order parameters. The essence of the dynamics is an effective reduction by two units of the spatial dimension in the electron-hole pairing in the lowest Landau level (LLL) with energy $E=0$.[16–18] As we discuss below, there is however an essential difference between the QHE's in these two systems. While the pairing forces in monolayer graphene lead to a relativisticlike scaling $\Delta E \sim \sqrt{|eB|}$ for the dynamical gap, in bilayer graphene, such a scaling should take place only for strong magnetic fields, $B \gtrsim B_{thr}$, where the threshold magnetic field is estimated as $B_{thr} \sim 30$ T (see Sec. III B). For $B \lesssim B_{thr}$, a nonrelativisticlike scaling $\Delta E \sim |eB|$ is realized in the bilayer. The origin of this phenomenon is very different forms of the polarization function in monolayer graphene and bilayer one that in turn is determined by the different dispersion relations for quasiparticles in these two systems.

The polarization function is one of the major players in the QHE in bilayer graphene. As will be shown below, its role is important because it is proportional to the large mass of quasiparticles, $m \sim 10^{-2} m_e \sim 10^8 \mathrm{K}/c^2 \gg \hbar^2/e^2 l$ unless $B \gtrsim 30$ T, which leads to strong screening.

Using the random phase approximation (RPA) in the analysis of the gap equation, we found two competing solutions: (I) a ferromagnetic (spin splitting) solution and (II) a layer asymmetric solution, actively discussed in the literature. Studying how the energy gaps of these solutions depend on the longitudinal component $B_\parallel$ of the magnetic field at a fixed value of the transverse component $B_\perp$, we found that while the gap of the solution I increases with $B_\parallel$, the gap of the solution II decreases as $B_\parallel$ increases. Comparing this behavior with that observed in experiment in Ref. 6 and calculating the energy density of the ground states for these solutions, we come to the following scenario. While at low magnetic fields, the layer asymmetric solution II is realized with the energy gap $\Delta E \sim 10B$ [T]K, there exists a first-order phase transition to the ferromagnetic phase corresponding to the solution I at some critical value $B_{cr}$. The experiment[6] implies that the value of $B_{cr}$ satisfies $B_{cr} \gtrsim 10$ T for $B_\parallel=0$. The phase diagram in the plane $(\tilde{\Delta}_0, B)$, where $\tilde{\Delta}_0$ is a top-bottom gates voltage imbalance, is described.

The paper is organized as follows. In Sec. II, the Hamiltonian of the model, its symmetries and order parameters are described. In Sec. III, by using the Baym-Kadanoff formalism,[19] the gap equation for the quasiparticle propagator including the polarization function is derived and the properties of the polarization function are described. In Sec. IV A, the properties of the solutions of the gap equations and

 

the phase diagram of the model are discussed. In Sec. IV B, we compare our results with experiment. In Sec. V, we summarize the main results of the paper. In Appendix, a detailed derivation of the polarization function in a magnetic field in bilayer graphene is presented.

## II. MODEL

### A. Hamiltonian

The free part of the effective low-energy Hamiltonian of bilayer graphene is[1]

$$H_0 = -\frac{1}{2m}\int d^2x \Psi^+_{Vs}(x)\begin{pmatrix} 0 & (\pi^\dagger)^2 \\ \pi^2 & 0 \end{pmatrix}\Psi_{Vs}(x), \qquad (1)$$

where $\pi = \hat{p}_{x_1} + i\hat{p}_{x_2}$ and the canonical momentum $\hat{\mathbf{p}} = -i\hbar\nabla + e\mathbf{A}/c$ includes the vector potential $\mathbf{A}$ corresponding to the external magnetic field $\mathbf{B}$. Without magnetic field, this Hamiltonian generates the spectrum $E = \pm\frac{p^2}{2m}$, $m = \gamma_1/2v_F^2$, where the Fermi velocity $v_F \simeq c/300$ and $\gamma_1 \approx 0.34-0.40$ eV. The two component spinor field $\Psi_{Vs}$ carries the valley ($V = K, K'$) and spin ($s = +, -$) indices. We will use the standard convention: $\Psi^T_{Ks} = (\psi_{A1}, \psi_{B2})_{Ks}$ whereas $\Psi^T_{K's} = (\psi_{B2}, \psi_{A1})_{K's}$. Here $A_1$ and $B_2$ correspond to those sublattices in the layers 1 and 2, respectively, which, according to Bernal ($A_2 - B_1$) stacking, are relevant for the low-energy dynamics. The effective Hamiltonian (1) is valid for magnetic fields $1\ \mathrm{T} < B < B_{thr}$. For $B < 1$ T, the trigonal warping should be taken into account.[1] For $B > B_{thr}$, a monolayerlike Hamiltonian with linear dispersion should be used.

The Zeeman and Coulomb interactions plus a top-bottom gates voltage imbalance $\tilde{\Delta}_0$ in bilayer graphene are described as (henceforth we will omit indices $V$ and $s$ in the field $\Psi_{Vs}$)

$$H_{int} = \mu_B B\int d^2x \Psi^+(x)\sigma_3\Psi(x) + \frac{e^2}{2\kappa}\int d^3x d^3x' \frac{n(\mathbf{x})n(\mathbf{x}')}{|\mathbf{x}-\mathbf{x}'|} + \tilde{\Delta}_0\int d^2x \Psi^+(x)\xi\tau_3\Psi(x), \qquad (2)$$

where $\mu_B$ is the Bohr magneton, $\sigma_3$ is a spin matrix, $\kappa$ is the dielectric constant, and $n(\mathbf{x}) = \delta(z-\frac{d}{2})\rho_1(x) + \delta(z+\frac{d}{2})\rho_2(x)$ is the three-dimensional charge density ($d \simeq 0.35$ nm is the distance between the two layers). The Pauli matrix $\tau_3$ in the voltage imbalance term acts on layer components, and $\xi = \pm 1$ for the valleys $K$ and $K'$, respectively.

Integrating over $z$ and $z'$ in this equation, one can rewrite $H_{int}$ as

$$H_{int} = \mu_B B\int d^2x \Psi^+(x)\sigma_3\Psi(x) + \frac{1}{2}\int d^2x d^2x' \times[V(x-x')(\rho_1(x)\rho_1(x') + \rho_2(x)\rho_2(x')) + 2V_{12}(x-x')\rho_1(x)\rho_2(x')] + \tilde{\Delta}_0\int d^2x \Psi^+(x)\xi\tau_3\Psi(x). \qquad (3)$$

Here the potential $V(x)$ describes the intralayer interactions and, therefore, coincides with the bare potential in monolayer graphene whose Fourier transform is given by $\tilde{V}(k) = 2\pi e^2/\kappa k$. The potential $V_{12}$ describes the interlayer electron interactions. Its Fourier transform is $\tilde{V}_{12}(k) = (2\pi e^2/\kappa)(e^{-kd}/k)$. The two-dimensional charge densities $\rho_1(x)$ and $\rho_2(x)$ are

$$\rho_1(x) = \Psi^+(x)P_1\Psi(x), \quad \rho_2(x) = \Psi^+(x)P_2\Psi(x), \qquad (4)$$

where $P_1 = \frac{1+\xi\tau^3}{2}$ and $P_2 = \frac{1-\xi\tau^3}{2}$ are projectors on states in the layers 1 and 2, respectively. When the polarization effects are taken into account, the potentials $V(x)$ and $V_{12}(x)$ are replaced by effective interactions $V_{eff}(x)$ and $V_{12\,eff}(x)$, respectively, whose Fourier transforms are given in Eqs. (A3) and (A4) in Appendix.

### B. Symmetries and order parameters

The Hamiltonian $H = H_0 + H_{int}$, with $H_0$ and $H_{int}$ in Eqs. (1) and (3), describes the dynamics at the neutral point (with no doping). Because of the projectors $P_1$ and $P_2$ in charge densities in Eq. (4), the symmetry of the Hamiltonian $H$ is essentially lower than the symmetry in monolayer graphene. If both the Zeeman and $\tilde{\Delta}_0$ terms are ignored, it is $\mathrm{U}^{(K)}(2)_S \times \mathrm{U}^{(K')}(2)_S \times Z_{2V}^{(+)} \times Z_{2V}^{(-)}$, where $\mathrm{U}^{(V)}(2)_S$ defines the U(2) spin transformations in a fixed valley $V = K, K'$, and $Z_{2V}^{(s)}$ describes the valley transformation $\xi \to -\xi$ for a fixed spin $s = \pm$ [recall that in monolayer graphene the symmetry would be U(4) (Ref. 18)]. The Zeeman interaction lowers this symmetry down to $G_2 \equiv U^{(K)}(1)_+ \times U^{(K)}(1)_- \times U^{(K')}(1)_+ \times U^{(K')}(1)_- \times Z_{2V}^{(+)} \times Z_{2V}^{(-)}$, where $\mathrm{U}^{(V)}(1)_s$ is the U(1) transformation for fixed values of both valley and spin. Recall that the corresponding symmetry in monolayer graphene is $G_1 \equiv \mathrm{U}^{(+)}(2)_V \times \mathrm{U}^{(-)}(2)_V$, where $\mathrm{U}^{(s)}(2)_V$ is the U(2) valley transformations for a fixed spin. Including the $\tilde{\Delta}_0$ term lowers the $G_2$ symmetry further down to the $\bar{G}_2 \equiv \mathrm{U}^{(K)}(1)_+ \times \mathrm{U}^{(K)}(1)_- \times \mathrm{U}^{(K')}(1)_+ \times \mathrm{U}^{(K')}(1)_-$.

Although the $G_1$ and $G_2$ symmetries are quite different, it is noticeable that their spontaneous breakdowns can be described by the same QHF and MC order parameters. The point is that these $G_1$ and $G_2$ define the same four conserved commuting currents whose charge densities (and four corresponding chemical potentials) span the QHF order parameters (we use the notations of Ref. 15)

$$\mu_s:\ \langle\Psi^\dagger_s\Psi_s\rangle = \langle\psi^\dagger_{KA_1s}\psi_{KA_1s} + \psi^\dagger_{K'A_1s}\psi_{K'A_1s} + \psi^\dagger_{KB_2s}\psi_{KB_2s} + \psi^\dagger_{K'B_2s}\psi_{K'B_2s}\rangle, \qquad (5)$$

$$\tilde{\mu}_s:\ \langle\Psi^\dagger_s\xi\Psi_s\rangle = \langle\psi^\dagger_{KA_1s}\psi_{KA_1s} - \psi^\dagger_{K'A_1s}\psi_{K'A_1s} + \psi^\dagger_{KB_2s}\psi_{KB_2s} - \psi^\dagger_{K'B_2s}\psi_{K'B_2s}\rangle. \qquad (6)$$

The order parameter in Eq. (5) is the charge density for a fixed spin whereas the order parameter in Eq. (6) determines the charge-density imbalance between the two valleys. The corresponding chemical potentials are $\mu_s$ and $\tilde{\mu}_s$, respectively. While the former order parameter preserves the $G_2$ symmetry, the latter completely breaks its discrete subgroup $Z_{2V}^{(s)}$. Their MC cousins are

$$\Delta_s:\ \langle \Psi_s^\dagger \tau_3 \Psi_s\rangle = \langle \psi^\dagger_{KA_1s}\psi_{KA_1s} - \psi^\dagger_{K'A_1s}\psi_{K'A_1s} - \psi^\dagger_{KB_2s}\psi_{KB_2s} + \psi^\dagger_{K'B_2s}\psi_{K'B_2s}\rangle, \tag{7}$$

$$\tilde{\Delta}_s:\ \langle \Psi_s^\dagger \xi\tau_3 \Psi_s\rangle = \langle \psi^\dagger_{KA_1s}\psi_{KA_1s} + \psi^\dagger_{K'A_1s}\psi_{K'A_1s} - \psi^\dagger_{KB_2s}\psi_{KB_2s} - \psi^\dagger_{K'B_2s}\psi_{K'B_2s}\rangle. \tag{8}$$

These order parameters can be rewritten in the form of Dirac mass terms.[15] The corresponding masses are $\Delta_s$ and $\tilde{\Delta}_s$, respectively. While the order parameter in Eq. (7) preserves the $G_2$, it is odd under time reversal $\mathcal{T}$.[20] On the other hand, the order parameter in Eq. (8), connected with the conventional Dirac mass $\tilde{\Delta}$, determines the charge-density imbalance between the two layers.[1] Like the QHF order parameter in Eq. (6), this mass term completely breaks the $Z_{2V}^{(s)}$ symmetry and is even under $\mathcal{T}$. Let us emphasize that unlike a spontaneous breakdown of continuous symmetries, a spontaneous breakdown of the discrete valley symmetry $Z_{2V}^{(s)}$, with the order parameters $\langle \Psi_s^\dagger \xi \Psi_s\rangle$ and $\langle \Psi_s^\dagger \xi\tau_3 \Psi_s\rangle$, is not forbidden by the Mermin-Wagner theorem at finite temperatures in a planar system.[21]

Note that because of the Zeeman interaction, the $\mathrm{SU}^{(V)}(2)_S$ is explicitly broken, leading to a spin gap. This gap could be dynamically strongly enhanced.[22] In that case, a quasispontaneous breakdown of the $\mathrm{SU}^{(V)}(2)_S$ takes place. The corresponding ferromagnetic phase is described by the chemical potential $\mu_3=(\mu_+-\mu_-)/2$, corresponding to the QHF order parameter $\langle \Psi^\dagger \sigma_3 \Psi\rangle$, and by the mass $\Delta_3=(\Delta_+ - \Delta_-)/2$ corresponding to the MC order parameter $\langle \Psi^\dagger \tau_3\sigma_3 \Psi\rangle$.[15]

## III. GAP EQUATION

### A. General remarks

In this section, in the framework of the Baym-Kadanoff formalism,[19] and using the polarization function calculated in the RPA, we derive and analyze the gap equation for the LLL quasiparticle propagator with the order parameters introduced above. Recall that in bilayer graphene, the LLL includes both the $n=0$ and $n=1$ Landau levels (LLs), if the Coulomb interaction is ignored.[1] Therefore there are sixteen parameters $\mu_s(n)$, $\Delta_s(n)$, $\tilde{\mu}_s(n)$, and $\tilde{\Delta}_s(n)$ with $n=0,1$.

As will be shown below, including the polarization function in the description of the LLL dynamics is necessary. The point is that this function is proportional to a large mass of quasiparticles, $m\sim 10^{-2}m_e\sim 10^8$ K$/c^2 \gg \hbar^2/e^2 l$ unless $B \gtrsim 30$ T, which leads to strong screening effects.

It will be shown below that the region of relevant values of wave vector $\mathbf{k}$ in the gap equation for the LLL states is $0<y\equiv \mathbf{k}^2 l^2/2 \lesssim 1$. While at small $y \ll 1$ the dominant contribution (around 80%) in the polarization function comes from the transitions between the LLL and the first higher LL with $n=2$, the number of the LLs providing relevant contributions in this function grows with increasing $y$ (for details, see the analysis in Appendix).

Last but not least, a characteristic scale in the bilayer dynamics in a magnetic field is the cyclotron energy $\hbar\omega_c \simeq 25.5B$ [T]K. The applicability of the LLL approximation for a quasiparticle propagator in the gap equation implies that the LLL energy gaps should be smaller than $\hbar\omega_c$. As we will see, this condition is fulfilled in bilayer graphene.

### B. Analysis of the gap equation

The effective action in the Baym-Kadanoff formalism in two-loop approximation is a functional of the full Green's function $G$ and has the form

$$\begin{aligned}\Gamma(G) = &- i\,\mathrm{Tr}[\mathrm{Ln}G^{-1} + S^{-1}G - 1] \\ &- \int d^3u d^3u' \left\{ \frac{1}{2}\mathrm{tr}[G(u,u')G(u',u)]V_{eff}(u-u') \right. \\ &+ \mathrm{tr}[P_1 G(u,u')P_2 G(u',u)]V_{IL}(u-u') \\ &- \frac{1}{2}\mathrm{tr}[G(u,u)]\mathrm{tr}[G(u',u')]V_{eff}(u-u') \\ &\left. - \mathrm{tr}[P_1 G(u,u)]\mathrm{tr}[P_2 G(u',u')]V_{IL}(u-u') \right\},\end{aligned} \tag{9}$$

where $u\equiv(t,\mathbf{r})$, $t$ is the time coordinate and $\mathbf{r}=(x,y)$, $V_{IL}(u)=V_{12eff}(u)-V_{eff}(u)$ is the interlayer interaction, and the Fourier transforms of $V_{eff}(u)$ and $V_{12eff}(u)$ are given in Eqs. (A3) and (A4) in Appendix. Note that while here the trace Tr, the logarithm, and the product $S^{-1}G$ are taken in the functional sense, the trace tr runs over spinor and spin indices.

The stationary condition $\delta\Gamma(G)/\delta G=0$ leads to the gap (Schwinger-Dyson) equation in mean field approximation, which will be written in the form convenient in the presence of a magnetic field

$$\begin{aligned}G(u_1,u_2) = S(u_1,u_2) &+ i\int d^3u_1' d^3u_2' S(u_1,u_1')G(u_1',u_2') \\ &\times G(u_2',u_2)V_{eff}(u_1'-u_2') + i\int d^3u_1' d^3u_2' S(u_1,u_1') \\ &\times [P_1 G(u_1',u_2')P_2 + P_2 G(u_1',u_2')P_1]G(u_2',u_2) \\ &\times V_{IL}(u_1'-u_2') - i\int d^3u_2' S(u_1,u_2') \\ &\times \{\mathrm{tr}[G(u_1,u_1)]\tilde{V}_{eff}(0) + (P_1\,\mathrm{tr}[P_2 G(u_1,u_1)] \\ &+ P_2\,\mathrm{tr}[P_1 G(u_1,u_1)]) \\ &\times \tilde{V}_{IL}(0)\}G(u_2',u_2),\end{aligned} \tag{10}$$

where $\tilde{V}_{eff}(0)$ and $\tilde{V}_{IL}(0)$ are the Fourier transforms of $V_{eff}(u)$ and $V_{IL}(u)$ taken at $\omega=\mathbf{k}=0$.

We will use the Landau gauge for a two-dimensional vector potential, $\mathbf{A}_\parallel=(0,B_\perp x)$, where $B_\perp$ is the component of the magnetic field $\mathbf{B}$ orthogonal to the $xy$ plane of graphene. Then, the free Green's function $S(u_1,u_2)$ can be written as a product of a translation invariant part $\tilde{S}(u_1-u_2)$ times the Schwinger phase factor[16,23]

$$S(u_1,u_2)=\exp\left[-i\frac{(x_1+x_2)(y_1-y_2)}{2l^2}\right]\widetilde{S}(u_1-u_2). \quad (11)$$

After extracting the Schwinger phase factor in the full propagator

$$G(u_1,u_2)=\exp\left[-i\frac{(x_1+x_2)(y_1-y_2)}{2l^2}\right]\widetilde{G}(u_1-u_2) \quad (12)$$

and making the Fourier transform with respect to $t$, we get the following equation for the translation invariant part $\widetilde{G}$:

$$\begin{aligned}\widetilde{G}(\Omega,\mathbf{r})=\widetilde{S}(\Omega,\mathbf{r})+i\int\frac{d\omega}{2\pi}\int d^2\mathbf{r}_1'd^2\mathbf{r}_2'e^{i[(x-x_2')y_1'-(y-y_2')x_1']/2l^2}\\ \times\widetilde{S}(\Omega,\mathbf{r}-\mathbf{r}_1')[\widetilde{G}(\omega,\mathbf{r}_1'-\mathbf{r}_2')V_{eff}(\Omega-\omega,\mathbf{r}_1'-\mathbf{r}_2')\\ +(P_1\widetilde{G}(\omega,\mathbf{r}_1'-\mathbf{r}_2')P_2+P_2\widetilde{G}(\omega,\mathbf{r}_1'-\mathbf{r}_2')P_1)V_{IL}\\ \times(\Omega-\omega,\mathbf{r}_1'-\mathbf{r}_2')]\widetilde{G}(\Omega,\mathbf{r}_2')-i\int d^2\mathbf{r}_2'e^{i[xy_2'-yx_2']/2l^2}\\ \times\widetilde{S}(\Omega,\mathbf{r}-\mathbf{r}_2')\{\mathrm{tr}[\widetilde{G}(0)]\widetilde{V}_{eff}(0)+(P_1\ \mathrm{tr}[P_2\widetilde{G}(0)]\\ +P_2\ \mathrm{tr}[P_1\widetilde{G}(0)])\widetilde{V}_{IL}(0)\}\widetilde{G}(\Omega,\mathbf{r}_2'), \quad (13)\end{aligned}$$

where $\mathbf{r}=\mathbf{r}_1-\mathbf{r}_2$.

The translation invariant part of the free propagator can be expanded over the LLs (compare with Refs. 15 and 16)

$$\begin{aligned}\widetilde{S}_{\xi s}(\mathbf{r};\omega)=\frac{1}{2\pi l^2}\exp\left(-\frac{\mathbf{r}^2}{4l^2}\right)\sum_{n=0}^{\infty}\frac{1}{(\omega+i\delta\,\mathrm{sgn}\,\omega+\bar{\mu}_s)^2-E_n^2}\\ \times\left\{(\omega+\bar{\mu}_s+\xi\tau_3\widetilde{\Delta}_0)\left[P_-L_n\left(\frac{\mathbf{r}^2}{2l^2}\right)\right.\right.\\ \left.+P_+L_{n-2}\left(\frac{\mathbf{r}^2}{2l^2}\right)\right]+\frac{\hbar^2}{2ml^4}L_{n-2}^2\left(\frac{\mathbf{r}^2}{2l^2}\right)\\ \left.\times\begin{pmatrix}0 & (x-iy)^2\\ (x+iy)^2 & 0\end{pmatrix}\right\}, \quad (14)\end{aligned}$$

where $P_\pm=(1\pm\tau_3)/2$, $E_n=\sqrt{\hbar^2\omega_c^2n(n-1)+\widetilde{\Delta}_0^2}$, and $\omega_c=eB/mc$ is the cyclotron frequency, and the bare electron chemical potential $\bar{\mu}_s=\mu_0-sZ$ includes the Zeeman energy $Z\simeq\mu_BB=0.67B$ [T]K (the conventional chemical potential $\mu_0$, responsible for doping, is included for generality). The functions $L_n^\alpha(x)$ are generalized Laguerre polynomials, and by definition, $L_n(x)=L_n^0(x)$, $L_{-2}^\alpha(x)=L_{-1}^\alpha(x)\equiv0$.

For the LLL with $n=0,1$, expression (14) takes a simple form

$$\widetilde{S}_{\xi s}(\mathbf{r};\omega)=\frac{1}{2\pi l^2}\exp\left(-\frac{\mathbf{r}^2}{4l^2}\right)\left[L_0\left(\frac{\mathbf{r}^2}{2l^2}\right)+L_1\left(\frac{\mathbf{r}^2}{2l^2}\right)\right]S_{\xi s}(\omega)P_-, \quad (15)$$

where

$$S_{\xi s}(\omega)=\frac{1}{\omega+\bar{\mu}_s+\xi\widetilde{\Delta}_0+i\delta\,\mathrm{sgn}\,\omega}. \quad (16)$$

Motivated by expression (15) for the free propagator in the LLL approximation, we will use the following ansatz for the full propagator with the parameters $\mu_s(n)$, $\tilde{\mu}_s(n)$, $\Delta_s(n)$, and $\widetilde{\Delta}_s(n)$ related to the order parameters in Eqs. (5)–(8)

$$\begin{aligned}\widetilde{G}_{\xi s}(\mathbf{r};\omega)=\frac{1}{2\pi l^2}\exp\left(-\frac{\mathbf{r}^2}{4l^2}\right)\left[G_{\xi s0}(\omega)L_0\left(\frac{\mathbf{r}^2}{2l^2}\right)\right.\\ \left.+G_{\xi s1}(\omega)L_1\left(\frac{\mathbf{r}^2}{2l^2}\right)\right]P_-, \quad (17)\end{aligned}$$

where

$$G_{\xi sn}(\omega)=\frac{1}{\omega-E_{\xi ns}+i\delta\,\mathrm{sgn}\,\omega} \quad (18)$$

and

$$E_{\xi ns}=-[\mu_s(n)+\Delta_s(n)]+\xi[\tilde{\mu}_s(n)-\widetilde{\Delta}_s(n)],\quad n=0,1 \quad (19)$$

are the energies of the LLL states depending on the order parameters $\mu_s(n),\tilde{\mu}_s(n),\Delta_s(n),\widetilde{\Delta}_s(n)$.

Inserting the ansatz in Eq. (17) into Eq. (13) and using the orthogonality of the Laguerre polynomials, we derive the following system of equations for the functions $G_{\xi sn}(\omega)$:

$$\begin{aligned}G_{\xi s0}^{-1}(\Omega)=S_{\xi s}^{-1}(\Omega)-i\int\frac{d\omega d^2k}{(2\pi)^3}[G_{\xi s0}(\omega)\\ +G_{\xi s1}(\omega)\mathbf{k}^2l^2/2]e^{-\mathbf{k}^2l^2/2}\widetilde{V}_{eff}(\Omega-\omega,|\mathbf{k}|)\\ +\frac{1}{4\pi l^2}\left(\frac{1+\xi}{2}A_1+\frac{1-\xi}{2}A_2\right)\widetilde{V}_{IL}(0), \quad (20)\end{aligned}$$

$$\begin{aligned}G_{\xi s1}^{-1}(\Omega)=S_{\xi s}^{-1}(\Omega)-i\int\frac{d\omega d^2k}{(2\pi)^3}[G_{\xi s0}(\omega)\mathbf{k}^2l^2/2+G_{\xi s1}(\omega)\\ \times(1-\mathbf{k}^2l^2/2)^2]e^{-\mathbf{k}^2l^2/2}\widetilde{V}_{eff}(\Omega-\omega,|\mathbf{k}|)\\ +\frac{1}{4\pi l^2}\left(\frac{1+\xi}{2}A_1+\frac{1-\xi}{2}A_2\right)\widetilde{V}_{IL}(0). \quad (21)\end{aligned}$$

Here $A_1=\Sigma_{n,s}\mathrm{sgn}(E_{-ns})$ and $A_2=\Sigma_{n,s}\mathrm{sgn}(E_{+ns})$. The second and third terms on right-hand sides of Eqs. (20) and (21) describe the Fock and Hartree interactions, respectively. Note that because for the LLL states only the component $\psi_{B_2s}$ ($\psi_{A_1s}$) of the wave function at the $K(K')$ valley is nonzero, their energies depend only on the eight independent combinations of the QHF and MC parameters shown in Eq. (19).

As is shown in Appendix, neglecting the dependence on $d$ in the function $\widetilde{V}_{eff}(\omega,k)$ describing the exchange interactions, one gets

$$\widetilde{V}_{eff}(\omega,k)=\frac{2\pi e^2}{\kappa}\frac{1}{k+\frac{4\pi e^2}{\kappa}\Pi(\omega,\mathbf{k}^2)} \quad (22)$$

with $\Pi(\omega,k^2)\equiv\Pi_{11}(\omega,\mathbf{k})+\Pi_{12}(\omega,\mathbf{k})$, where the polarization function $\Pi_{ij}$ describes electron densities correlations on the

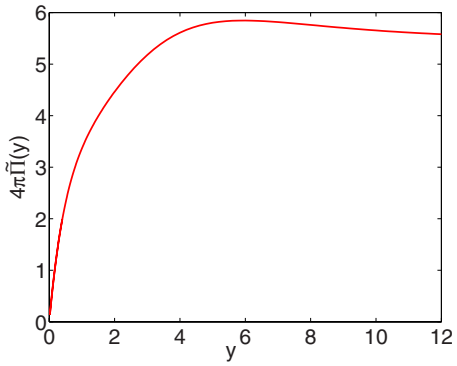


FIG. 1. (Color online) The static polarization function $4\pi\tilde{\Pi}(y)$.

layers $i$ and $j$ in a magnetic field [see Eqs. (A5), (A8), and (A9)]. As to the Hartree interactions, it is [see Eq. (A7)]

$$\tilde{V}_{IL}(\omega=0,k=0)=-\frac{2\pi e^2 d}{\kappa_{eff}},$$

$$\kappa_{eff}=\kappa+2\pi e^2 d[\Pi_{11}(0)-\Pi_{12}(0)]. \tag{23}$$

It is estimated in Appendix that the value of the dynamical part of $\kappa_{eff}$, i.e., $\kappa_{eff}-\kappa$, varies in the interval 1–4.

We utilize the frequency-independent order parameters $\mu,\tilde{\mu},\Delta,\tilde{\Delta}$ and take the external frequency $\Omega=0$ in Eqs. (20) and (21). The static approximation for the polarization function will be used, $\Pi(\omega,\mathbf{k}^2)\to\Pi(0,\mathbf{k}^2)$. As a justification of the latter, we present the following argument. Let us assume that the main contribution in the integrals over $\omega$ in Eqs. (20) and (21) comes from the pole terms in the functions $G_{\xi sn}(\omega)$ [see Eq. (18)]. The contribution of each pole in the polarization function has the form $\Pi(\omega=E_{\xi ns},\mathbf{k}^2)$, and the dependence on $E_{\xi ns}$ enters through $(E_{\xi ns}/\hbar\omega_c)^2$, where the cyclotron energy $\hbar\omega_c\simeq 25.5B$ [T]K. As will be shown below, the ratio $(E_{\xi ns}/\omega_c)^2$ is small, $\sim 0.15$, and, therefore, can be neglected in Eq. (A24), which leads to a static polarization function $\Pi(0,\mathbf{k}^2)$.

It is convenient to rewrite the static polarization $\Pi(0,\mathbf{k}^2)$ in the form $\Pi=(m/\hbar^2)\tilde{\Pi}(y)$, where both $\tilde{\Pi}$ and $y\equiv\mathbf{k}^2l^2/2$ are dimensionless. The function $\tilde{\Pi}(y)$ was expressed in terms of the sum over all the Landau levels [see Eq. (A25) in Appendix] and was analyzed both analytically and numerically. At $y\ll 1$, $\tilde{\Pi}(y)\simeq 0.55y$ and its derivative $\tilde{\Pi}'$ changes from 0.55 at $y=0$ to 0.12 at $y=1$. At large $y$ it approaches a zero magnetic field value, $\tilde{\Pi}(y)\simeq\ln 4/\pi$ (see Fig. 1).[24]

Because of the Gaussian factors $e^{-\mathbf{k}^2l^2/2}=e^{-y}$ in Eqs. (20) and (21), the relevant region in the integrals in these equations is $0<y\lesssim 1$. The crucial point in the analysis is that the region where the bare Coulomb term $k$ in the denominator of $V_{eff}(k)\equiv V_{eff}(0,k)$ Eq. (22) dominates is very small, $0<y\lesssim 10^{-3}B$ [T]. The main reason of that is a large mass of quasiparticles, $m\sim 10^{-2}m_e\sim 10^8\mathrm{K}/c^2\gg\hbar^2/e^2l$. The last inequality takes place unless $B\gtrsim 30$ T. As a result, the polarization function term dominates in $V_{eff}(k)$ that leads to $V_{eff}(k)$ of the form $V_{eff}(k)=C(y)\hbar^2/ml^2k^2$. The factor $\hbar^2/ml^2k^2$ has the same $k$ dependence as the Coulomb potential in two dimensions and the factor $C(y)$ describes its smooth modulations at $0\le y\lesssim 1$ (see Fig. 1). It is unlike the case of monolayer graphene where the effective interaction is proportional to $1/k$.

By using the change of variables $\mathbf{k}\to l\mathbf{k}$ in Eqs. (20) and (21), one can see that $|eB|$ occurs as an overall factor in the front of the integrals in these equations. The latter leads to the scaling $\Delta E\sim|eB|$ for the dynamical energy gap and not $\Delta E\sim\sqrt{|eB|}$ taking place in monolayer graphene[8,9,15] (see Sec. IV A below).

As shown in Appendix, the contribution of the LLL with $n=0,1$ in the polarization function is identically zero. At $y\ll 1$, the main contribution (around 80%) comes from the transitions between the LLL and the first higher LL with $n=2$. With increasing $y$, the number of higher LLs providing relevant contributions in the polarization function grows.

As to the condition of the applicability of this low-energy model, according to Ref. 1, it is determined by the relation $\hbar\omega_c\sqrt{n(n-1)}\le\gamma_1/4$. Its left-hand side is nonzero for $n\ge 2$ and increases linearly with $B$. Taking $n=2$ and the sign of equality in this relation, we find the threshold magnetic field $B_{thr}=\frac{45}{\sqrt{2}}$ T$\approx 32$ T that determines the upper limit for the values of $B$ for which the low-energy model is applicable.

With the static polarization function, the integration over the frequency $\omega$ in Eqs. (20) and (21) can be performed explicitly, and we get a system of algebraic equations for the energies $E_{\xi ns}$ in Eq. (19)

$$-E_{\xi 0s}=\mu_0-sZ+\xi\tilde{\Delta}_0-\frac{1}{2ml^2}[\mathrm{sgn}(E_{\xi 0s})I_1(x)+\mathrm{sgn}(E_{\xi 1s})I_2(x)]+\frac{1}{4\pi l^2}\left[(A_1+A_2)V_{eff}(0)+\left(\frac{1-\xi}{2}A_2+\frac{1+\xi}{2}A_1\right)V_{IL}(0)\right], \tag{24}$$

$$-E_{\xi 1s}=\mu_0-sZ+\xi\tilde{\Delta}_0-\frac{1}{2ml^2}[\mathrm{sgn}(E_{\xi 0s})I_2(x)+\mathrm{sgn}(E_{\xi 1s})I_3(x)]+\frac{1}{4\pi l^2}\left[(A_1+A_2)V_{eff}(0)+\left(\frac{1-\xi}{2}A_2+\frac{1+\xi}{2}A_1\right)V_{IL}(0)\right], \tag{25}$$

where the quantities $I_i(x)$ are

$$I_i(x)=\int_0^\infty\frac{dyf_i(y)e^{-y}}{\kappa\sqrt{xy}+4\pi\tilde{\Pi}(y)} \tag{26}$$

with $f_i(y)=[1,y,(1-y)^2]$ for $i=1,2,3$, respectively. Here the dimensionless variable $x=2\hbar^4/e^4m^2l^2=(4\hbar\omega_c/\alpha^2\gamma_1)(v_F/c)^2\simeq 0.003B$ [T], where $\alpha=1/137$ is the fine-structure constant and we used the values $\gamma_1=0.39$ eV, $\hbar\omega_c=\hbar^2/ml^2=2.19B$ [T]meV, $v_F=8.0\times 10^5$ m/s (see Ref. 1).

## IV. SOLUTIONS AND PHASE DIAGRAM: THEORY AND EXPERIMENT

### A. Properties of solutions

In this section the solutions of Eqs. (24) and (25) and the phase diagram of the system these solutions lead to will be described. If the Zeeman term is ignored, the equations for parameters with different spin indices coincide. If the voltage imbalance $\tilde{\Delta}_0$ term is absent, these equations are also invariant with respect to the permutation of layer indices ($\xi \to -\xi$) [note that $A_1 \leftrightarrow A_2$ under the change $\xi \to -\xi$]. Clearly, these symmetries of the gap equations are due to the $\mathrm{SU}^{(K)}(2)_S \times \mathrm{SU}^{(K')}(2)_S \times Z_{2V}^{(+)} \times Z_{2V}^{(-)}$ symmetry of the bilayer Hamiltonian discussed in Sec. II B [note that if the interlayer Coulomb interaction term $V_{IL}$ were absent, we would have the U(4) symmetry group, as in monolayer graphene].

Due to the Zeeman and $\tilde{\Delta}_0$ terms, these equations are inhomogeneous. It is natural to expect that the lowest-energy solution will have the sign correlating with the sign of inhomogeneous terms (solutions with different signs are degenerate in the case of homogeneous equations). Without loss of generality, we can assume that $\tilde{\Delta}_0$ is positive.

At the neutrality point ($\mu_0=0$ and $A_1+A_2=0$), we found two competing solutions of these equations: (I) a ferromagnetic (spin splitting) solution and (II) a layer asymmetric solution, actively discussed in the literature. The energy in Eq. (19) of the LLL states of the solution I equals

$$E_{\xi ns}^{(I)} = s\left[Z + \frac{\hbar^2}{2ml^2}F_n(x)\right] - \xi\tilde{\Delta}_0, \tag{27}$$

where $F_0(x)=I_1(x)+I_2(x)$ and $F_1(x)=I_2(x)+I_3(x)$ with $I_i$ in Eq. (26). The solution exists for $\tilde{\Delta}_0 < Z+\frac{\hbar^2}{2ml^2}F_1(x)$. Since $A_1=A_2=0$ in this solution, the Hartree interaction does not contribute in $E_{\xi ns}^{(I)}$. Note that the dynamical term $(\hbar^2/2ml^2)F_n(x)$ in Eq. (27) can be rewritten as $(\hbar|eB|/2mc)F_n(x)$, where $F_n(x)$ depends on $B$ logarithmically for $x \ll 1$.

The energy in Eq. (19) of the LLL states of the solution II is different

$$E_{\xi ns}^{(II)} = sZ - \xi\left[\tilde{\Delta}_0 + \frac{\hbar^2}{2ml^2}F_n(x) - \frac{2e^2d}{\kappa_{eff}l^2}\right]. \tag{28}$$

The last term in the square brackets is the Hartree one and the solution exists for $\tilde{\Delta}_0 > \frac{2e^2d}{\kappa_{eff}l^2} + Z - \frac{\hbar^2}{2ml^2}F_1(x)$. For illustrative purpose, in suspended bilayer graphene, with $\kappa \sim 1$, we will use $\kappa_{eff}=4$ [see Eq. (23)].

The energy density of the ground state for these solutions is ($a$=I,II)

$$\epsilon^{(a)} = -\frac{1}{8\pi l^2}\sum_{\xi=\pm}\sum_{s=\pm}\sum_{n=0,1}\left[|E_{\xi ns}^{(a)}| + (-s0.67B + \xi\tilde{\Delta}_0)\mathrm{sgn}\, E_{\xi ns}^{(a)}\right]. \tag{29}$$

It is easy to check that for balanced bilayer ($\tilde{\Delta}_0=0$) the solution I is favorite. There are two reasons of that: the presence of the Zeeman term and the capacitor like Hartree contribution in the energy $E_{\xi ns}^{(\mathrm{II})}$ in the solution II.

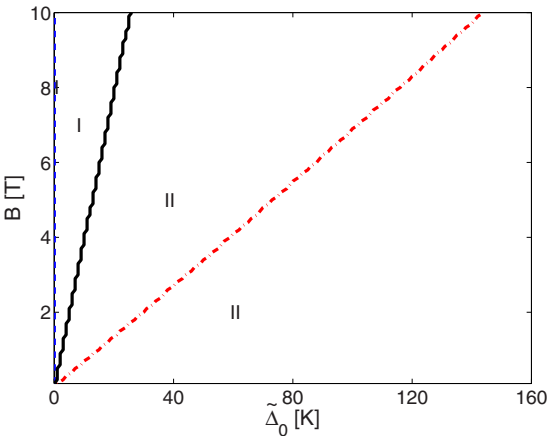


FIG. 2. (Color online) The phase diagram in the $(\tilde{\Delta}_0, B)$ plane at $B_\parallel=0$. Here the effective $\kappa_{eff}=4$.

In Fig. 2, the phase diagram on the plane $(\tilde{\Delta}_0, B)$, at $B_\parallel=0$, is presented. The I (II) area is that where the solution I (solution II) is favorite. The two dashed lines compose the boundary of the region where the two solutions coexist [the solution I does not exist to the right of the (red) dashed line in the region II while the solution II does not exist to the left of the (blue) dashed line in the region I]. The black bold line is a line of a phase transition between the phases I and II. Because the solutions coexist in the region around that line, the phase transition is a first-order one. The equation for the critical value $B_{cr}$ has a simple form, $B_{cr}$ [T] $\simeq 0.4\tilde{\Delta}_0$ [K].

It is noticeable that for any fixed value of $B(\tilde{\Delta}_0)$, there are sufficiently large values of $\tilde{\Delta}_0$ ($B$), at which the solution I (solution II) does not exist at all. It is because a voltage imbalance (Zeeman term) tends to destroy the solution I (solution II).

For $\tilde{\Delta}_0=0$, the dependence of the LLL energies $E_{\xi ns}^{(\mathrm{I})}$ of the solution I on $B$, at $B_\parallel=0$, is shown on the left panel in Fig. 3 (the LLL states with opposite $\xi$ remain degenerate in this solution). The perfectly linear form of this dependence is evident. Also, the degeneracy between the states of the $n=0$ LL and those of the $n=1$ LL is removed. The energy gap corresponding to the $\nu=0$ plateau is $\Delta E^{(\mathrm{I})}=(E_{\xi 1+}^{(\mathrm{I})}-E_{\xi 1-}^{(\mathrm{I})})/2 \simeq 14.4B$ [T]K.

On the right panel in Fig. 3, the dependence of the LLL energies of the solution II on $B$, at $B_\parallel=0$, is shown for $\tilde{\Delta}_0=5$ K. It is also perfectly linear. Unlike the solution I, the LLL degeneracy is now completely removed. As to the energy gap corresponding to the $\nu=0$ plateau, it is $\Delta E^{(\mathrm{II})}=(E_{-1-}^{(\mathrm{II})}-E_{+1+}^{(\mathrm{II})})/2 \simeq 5$ K$+9.3B$ [T]K.

Figure 4 illustrates how the energy gaps of the two solutions depend on the longitudinal component of the magnetic field $B_\parallel=B\cos\alpha$ at a fixed value of the transverse component $B_\perp=B\sin\alpha$. As one can see, while the gap of the solution I increases with $B_\parallel$, the gap of the solution II decreases as $B_\parallel$ increases. These properties of course reflect the opposite roles of the Zeeman term in the dynamics of the solutions I and II.

Thus the results of the analysis of this subsection imply a possibility of the following two scenarios. When the top-

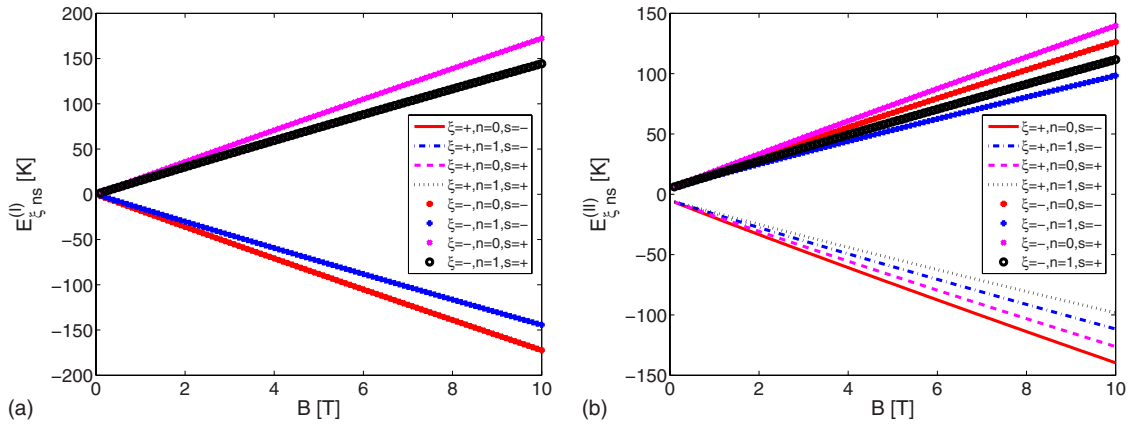


FIG. 3. (Color online) The LLL energies of the solutions I (left panel) and II (right panel) as functions of $B$ with $B_{\|}=0$. Here $\tilde{\Delta}_0=0$ and $\tilde{\Delta}_0=5$ K for solution I and solution II, respectively.

bottom gates voltage imbalance $\tilde{\Delta}_0=0$, the ferromagnetic phase I is favorite for all values of the magnetic field. For nonzero $\tilde{\Delta}_0$, the phase II is realized for the values magnetic fields up to the critical value $B_{cr}$, where a first-order phase transition to the ferromagnetic phase I takes place. As we will discuss in the next section, the experiment in Ref. 6 clearly prefers the second scenario.

What can be the origin of $\tilde{\Delta}_0$? As was pointed out in Ref. 6, it could be generated due to disorder-induced differences in carrier density between the top and bottom layers. A more interesting possibility is that a relatively small $\tilde{\Delta}_0$ is a dynamical parameter corresponding to spontaneous breakdown of the discrete valley symmetry $Z_{2V}^{(+)}\times Z_{2V}^{(-)}$ in bilayer graphene with no magnetic field.

### B. Comparison with experiment

The first experiments in bilayer graphene in a magnetic field[3,4] revealed quantum Hall states with the filling factor $\nu=\pm 4n$, $n=1,2,\ldots$ predicted in the framework of the one electron problem in Ref. 1. No traces of lifting the eightfold degeneracy of the LLL and the fourfold degeneracy of higher LLs were observed.

Recent experiments in bilayer graphene[6,7] showed the generation of energy gaps in a magnetic field resulting in complete lifting the eightfold degeneracy in the LLL, which leads to new quantum Hall states with filling factors $\nu=0,\pm 1,\pm 2,\pm 3$. While in Ref. 6 suspended bilayer graphene was used, bilayer graphene samples deposited on $SiO_2/Si$ substrates were used in Ref. 7. Because suspended bilayer graphene is much cleaner than that on a substrate, the new quantum Hall states in the former start to develop at essentially smaller magnetic fields than in the latter. Also, the energy gaps corresponding to these states are essentially larger in suspended samples than in those on substrates. Both these experiments clearly showed that the $\nu=0$ state is an insulating one.

Since in this paper the dynamics of the $\nu=0$ state in clean bilayer graphene is analyzed, it would be appropriate to compare our results with those in suspended graphene in more detail. The central results concerning the $\nu=0$ state in Ref. 6 are: (a) the observation of an extremely large magnetoresistance in the $\nu=0$ state due to the energy gap $\Delta E$, which scales linearly with a magnetic field $B$, $\Delta E \sim 3.5-10.5B_{\perp}$ [T]K at least for $B_{\perp}\lesssim 10$ T and (b) at fixed $B_{\perp}$, an increase in the parallel component of the field reduces the magnetoresistance at least for $B_{\perp}\lesssim 6$ T. This can be in-

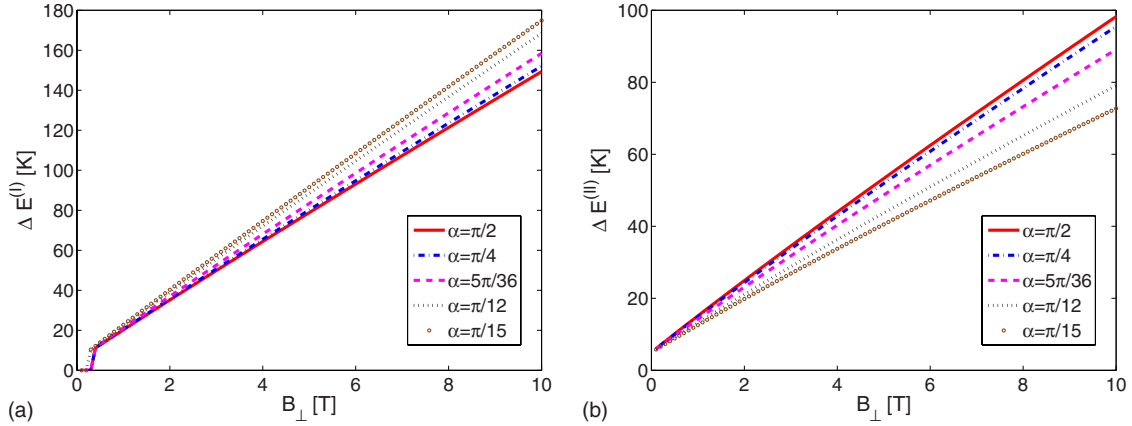


FIG. 4. (Color online) The dependence of the energy gaps of solutions I (left panel) and II (right panel) on the field $B_{\perp}$ for different angles. The parameter $\tilde{\Delta}_0=5$ K for both solutions I and II.

terpreted as reducing the energy gap $\Delta E$ with increasing $B_{\parallel}$.

As to result (a), the agreement of the expressions for both the gaps $\Delta E^{\mathrm{I}}$ and $\Delta E^{\mathrm{II}}$ derived in Sec. IV A with the gap $\Delta E$ observed in Ref. 6 is satisfactory. Concerning the result (b), it suggests that the longitudinal magnetic field suppresses the energy gap. This fact excludes the ferromagnetic phase as a candidate for the description of the clean bilayer graphene at least for $B_{\perp} \leq 6$ T (see left panel in Fig. 4). On the other hand, the solution II, describing the layer asymmetric phase, is a viable candidate for this role (see right panel in Fig. 4).

This conclusion together with the phase diagram in Fig. 1 suggests the following picture. At $B_{\perp} < B_{cr}$ with $B_{cr} \gtrsim 10$ T, the layer asymmetric phase (solution II) is realized. At $B_{\perp} = B_{cr}$, a phase transition to the ferromagnetic phase (solution I) takes place. Because these solutions coexist at $B_{\perp} < B_{cr}$, one should expect that it is a first-order phase transition. Taking literally the relation $B_{cr}\ [\mathrm{T}] \simeq 0.4\tilde{\Delta}_0\ [\mathrm{K}]$ derived from the phase diagram in Fig. 1 in Sec. IV A, we find that $B_{cr} \sim 10$ T corresponds to $\tilde{\Delta}_0 \sim 25$ K. However, because the existence of relevant dynamical contributions beyond the random phase approximation is quite possible, one should consider this relation just as a qualitative estimate.

## V. CONCLUSION

The dynamics of bilayer graphene in a magnetic field $B \lesssim B_{thr}$ is characterized by a very strong screening of the Coulomb interaction that relates to the presence of a large mass $m$ in the nonrelativisticlike dispersion relation for quasiparticles. The functional dependence of the gap on $B$ derived in Sec. IV A agrees with that obtained very recently in experiment in Ref. 6. The existence of the first-order phase transition between the layer asymmetric phase and the ferromagnetic one in the $(\tilde{\Delta}_0, B)$ plane is predicted.

There are still many open issues in this dynamics. In particular, (a) it would be important to include the chemical potential $\mu_0$ in the present analysis in order to describe the higher, $\nu = 1$, 2, and 3, LLL plateaus.[6,7] (b) The present ansatz with the 16 order parameters is the minimal one for describing the breakdown of the $\mathrm{U}^{(K)}(2)_S \times \mathrm{U}^{(K')}(2)_S \times Z_{2V}^{(+)} \times Z_{2V}^{(-)}$ symmetry in bilayer graphene. It could be extended in order to look for other solutions of the gap equation. A natural extension would be to include order parameters that mix the $n=0$ and $n=1$ LLL states. (c) Although in Sec. III B we presented arguments showing that the static limit for the polarization function is at least reasonable, it would be important to check this conclusion directly by analyzing the gap equation with a nonstatic polarization function. (d) It would be interesting to describe explicitly the dynamics around the threshold value $B_{thr}$, when the crossover between the regimes with the nonrelativisticlike scaling $\Delta E \sim |eB|$ and the relativisticlike one $\Delta E \sim \sqrt{|eB|}$ should take place. We are planning to consider these issues elsewhere.

## ACKNOWLEDGMENTS

We thank Junji Jia and S. G. Sharapov for fruitful discussions. The work of E.V.G and V.P.G. was supported partially by the SCOPES under Grant No. IZ73Z0_128026 of the Swiss NSF, under Grant No. SIMTECH 246937 of the European FP7 program, the joint Grant RFFR-DFFD No. F28.2/083 of the Russian Foundation for Fundamental Research (RFFR) and of the Ukrainian State Foundation for Fundamental Research (DFFD), and by the Program of Fundamental Research of the Physics and Astronomy Division of the NAS of Ukraine. The work of V.A.M. was supported by the Natural Sciences and Engineering Research Council of Canada.

## APPENDIX: POLARIZATION OPERATOR OF BILAYER GRAPHENE IN A MAGNETIC FIELD

The polarization function $\Pi_{ij}$ describes electron densities correlations on the layers $i$ and $j$

$$\delta(\omega+\omega')\delta(\mathbf{k}+\mathbf{k}')\Pi_{ij}(\omega,\mathbf{k}) = -i\langle 0|\rho_i(\omega,\mathbf{k}')\rho_j(\omega',\mathbf{k}')|0\rangle. \tag{A1}$$

There are two independent polarization functions, $\Pi_{11}=\Pi_{22}$ and $\Pi_{12}=\Pi_{21}$. Taking into account the polarization effects, the bare interactions transform into

$$\hat{V}_{eff} = \hat{V}\cdot\frac{1}{1+\hat{V}\cdot\hat{\Pi}} = \begin{pmatrix} \tilde{V}_{eff}(k) & \tilde{V}_{12eff}(k) \\ \tilde{V}_{12eff}(k) & \tilde{V}_{eff}(k) \end{pmatrix},$$

$$\hat{V} = \begin{pmatrix} \tilde{V}(k) & \tilde{V}_{12}(k) \\ \tilde{V}_{12}(k) & \tilde{V}(k) \end{pmatrix},$$

$$\hat{\Pi} = \begin{pmatrix} \Pi_{11}(k) & \Pi_{12}(k) \\ \Pi_{12}(k) & \Pi_{11}(k) \end{pmatrix}, \tag{A2}$$

with

$$\tilde{V}_{eff}(\omega,k) = \frac{2\pi e^2}{\kappa}\frac{k+\frac{2\pi e^2}{\kappa}\Pi_{11}(1-e^{-2kd})}{\left[k+\frac{2\pi e^2}{\kappa}(\Pi_{11}+\Pi_{12})(1+e^{-kd})\right]\left[k+\frac{2\pi e^2}{\kappa}(\Pi_{11}-\Pi_{12})(1-e^{-kd})\right]}, \tag{A3}$$

$$\tilde{V}_{12eff}(\omega,k)=\frac{2\pi e^2}{\kappa}\frac{ke^{-kd}-\frac{2\pi e^2}{\kappa}\Pi_{12}(1-e^{-2kd})}{\left[k+\frac{2\pi e^2}{\kappa}(\Pi_{11}+\Pi_{12})(1+e^{-kd})\right]\left[k+\frac{2\pi e^2}{\kappa}(\Pi_{11}-\Pi_{12})(1-e^{-kd})\right]}, \tag{A4}$$

where $k=|\mathbf{k}|$, and since $\Pi_{11}$ and $\Pi_{12}$ depend on $\omega$, the effective interactions $\tilde{V}_{eff}$ and $\tilde{V}_{12eff}$ depend on it too.

Neglecting the dependence on $d$ (i.e., taking $d=0$), we obtain

$$\tilde{V}_{eff}(\omega,k)=\tilde{V}_{12eff}(\omega,k)=\frac{2\pi e^2}{\kappa}\frac{1}{k+\frac{4\pi e^2}{\kappa}\Pi(\omega,k^2)}, \tag{A5}$$

where $\Pi(\omega,k^2)\equiv\Pi_{11}(\omega,\mathbf{k})+\Pi_{12}(\omega,\mathbf{k})$ is the polarization function in a magnetic field. On the other hand

$$\tilde{V}_{IL}(\omega,k)=\tilde{V}_{12eff}(\omega,k)-\tilde{V}_{eff}(\omega,k)=-\frac{2\pi e^2}{\kappa}\times\frac{1-e^{-kd}}{k+\frac{2\pi e^2}{\kappa}[\Pi_{11}(\omega,k)-\Pi_{12}(\omega,k)](1-e^{-kd})}. \tag{A6}$$

Therefore since the interlayer term $\tilde{V}_{IL}(\omega,k)$ appears in gap Eqs. (20) and (21) only at $\omega=k=0$, we find that

$$\tilde{V}_{IL}(\omega=0,k=0)=-\frac{2\pi e^2 d}{\kappa_{eff}},$$

$$\kappa_{eff}=\kappa+2\pi e^2 d[\Pi_{11}(0)-\Pi_{12}(0)]. \tag{A7}$$

By definition, the polarization functions $\Pi_{11}$ and $\Pi_{12}$ are defined as

$$\Pi_{11}(\omega,\mathbf{p})=i\int\frac{d\omega' d^2k}{(2\pi)^3}\mathrm{tr}[P_1\tilde{S}(\omega',\mathbf{k})P_1\tilde{S}(\omega+\omega',\mathbf{p}+\mathbf{k})], \tag{A8}$$

$$\Pi_{12}(\omega,\mathbf{p})=i\int\frac{d\omega' d^2k}{(2\pi)^3}\mathrm{tr}[P_1\tilde{S}(\omega',\mathbf{k})P_2\tilde{S}(\omega+\omega',\mathbf{p}+\mathbf{k})], \tag{A9}$$

where $P_1=(1+\xi\tau_3)/2$ and $P_2=(1-\xi\tau_3)/2$ are projectors on layers 1 and 2, respectively, the trace includes the summation both over the valley index $\xi$ and spin, and $\tilde{S}(\omega,\mathbf{k})$ is the Fourier transform of the translation invariant part of the free fermion propagator in Eq. (14) in a magnetic field.

We are interested in calculating the polarization function $\Pi(\omega,k^2)$ in the random phase approximation at the neutral point ($\mu_0=0$). Its expression in configuration space is

$$\Pi(\omega,\mathbf{r})=i\int\frac{d\omega'}{2\pi}\mathrm{tr}[P_1\tilde{S}(\omega',\mathbf{r})\tilde{S}(\omega+\omega',-\mathbf{r})], \tag{A10}$$

where a small Zeeman term in the fermion propagator will be ignored. Then

$$\begin{aligned}\Pi(\omega,\mathbf{p})&=\int d^2re^{-i\mathbf{pr}}\Pi(\omega,\mathbf{r})\\&=\frac{2i}{(2\pi l^2)^2}\sum_{n,m=0}^{\infty}\int\frac{d\omega'}{2\pi}\frac{1}{[\omega'^2-E_n^2+i0][(\omega+\omega')^2-E_m^2+i0]}\\&\times\int d^2re^{-\mathbf{r}^2/2l^2-i\mathbf{pr}}\Big\{(\omega'+\tilde{\Delta}_0)(\omega+\omega'+\tilde{\Delta}_0)[L_n(r^2/2l^2)L_m(r^2/2l^2)+L_{n-2}(r^2/2l^2)L_{m-2}(r^2/2l^2)]\\&+\frac{2\hbar^4r^4}{(2ml^4)^2}L_{n-2}^2(r^2/2l^2)L_{m-2}^2(r^2/2l^2)\Big\}.\end{aligned} \tag{A11}$$

Integrating over the angle and making the change of the variable $r^2=2l^2t$, we get

$$\begin{aligned}\Pi(\omega,\mathbf{p})&=\frac{i}{\pi l^2}\sum_{n,m=0}^{\infty}\int\frac{d\omega'}{2\pi}\frac{1}{[\omega'^2-E_n^2+i0][(\omega+\omega')^2-E_m^2+i0]}\int_0^{\infty}dte^{-t}J_0(\sqrt{2p^2l^2t})\{(\omega'+\tilde{\Delta}_0)(\omega+\omega'+\tilde{\Delta}_0)[L_n(t)L_m(t)\\&+L_{n-2}(t)L_{m-2}(t)]+2\omega_c^2t^2L_{n-2}^2(t)L_{m-2}^2(t)\},\end{aligned} \tag{A12}$$

where $J_\nu$ is a Bessel function and $E_n=\sqrt{\hbar^2\omega_c^2 n(n-1)+\tilde{\Delta}_0^2}$ [compare with Eq. (14)].

In order to evaluate the $t$ integral with the first term in the curl brackets in Eq. (A12), we will use the formula 7.422.2 in Ref. 25

$$\int_0^\infty dx x^{\nu+1} e^{-\alpha x^2} J_\nu(bx) L_m^{\nu-\sigma}(\alpha x^2) L_n^\sigma(\alpha x^2)$$
$$= (-1)^{m+n}(2\alpha)^{-\nu-1} b^\nu \times \exp\left(-\frac{b^2}{4\alpha}\right) L_m^{\sigma-m+n}\left(\frac{b^2}{4\alpha}\right) L_n^{\nu-\sigma+m-n}\left(\frac{b^2}{4\alpha}\right). \quad \text{(A13)}$$

Taking $\nu=\sigma=0, \alpha=1, b=2\sqrt{y}, y=p^2l^2/2$ in this expression, we obtain

$$\int_0^\infty dt e^{-t} J_0(2\sqrt{yt}) L_n(t) L_m(t) = (-1)^{m+n} e^{-y} L_m^{n-m}(y) L_n^{m-n}(y) \equiv (-1)^{m+n} e^{-y} I_{nm}(y) \quad \text{(A14)}$$

with

$$I_{nm}(y) = L_m^{n-m}(y) L_n^{m-n}(y). \quad \text{(A15)}$$

As $y\to 0$, we find

$$I_{nm}(y) \simeq \delta_{nm} - y[2n\delta_{nm} + (m+1)\delta_{n,m+1} + (n+1)\delta_{m,n+1}]. \quad \text{(A16)}$$

In order to evaluate the $t$ integral with the second term in the curl brackets in Eq. (A12)

$$\int_0^\infty dt t^2 e^{-t} J_0(2\sqrt{yt}) L_n^2(t) L_m^2(t) \equiv (-1)^{m+n} e^{-y} I_{nm}^{(2)}(y), \quad \text{(A17)}$$

we set $\nu=0, \sigma=2, b=2\sqrt{y}$ in Eq. (A13)

$$\int_0^\infty dx x e^{-x^2} J_0(2x\sqrt{y}) L_m^{-2}(x^2) L_n^2(x^2) = \frac{(-1)^{m+n}}{2} e^{-y} L_m^{2-m+n}(y) L_n^{-2+m-n}(y) \quad \text{(A18)}$$

and use the following identity for the Laguerre polynomials on the left-hand side of this equation:

$$L_l^k(x) = (-x)^{-k}\frac{(l+k)!}{l!} L_{l+k}^{-k}(x), \quad l \geq 0, k+l \geq 0. \quad \text{(A19)}$$

Then we arrive at

$$\int_0^\infty dt t^2 e^{-t} J_0(2\sqrt{yt}) L_{m-2}^2(t) L_n^2(t) = (-1)^{m+n}\frac{m!}{(m-2)!} e^{-y} L_m^{2+n-m}(y) L_n^{-2+m-n}(y) \quad \text{(A20)}$$

and therefore

$$I_{nm}^{(2)}(y) = (m+1)(m+2) L_{m+2}^{n-m}(y) L_n^{m-n}(y). \quad \text{(A21)}$$

Although the symmetry of $I_{nm}^{(2)}(y)$ under the interchange $n\leftrightarrow m$ is not explicit, it can be checked by using the identity in Eq. (A19). At small $y$, we get the following expansion for $I_{nm}^2(y)$:

$$I_{nm}^{(2)}(y) \simeq (n+1)(n+2)\delta_{nm} - y[2(n+1)^2(n+2)\delta_{nm} + \delta_{n,m+1} n(n+1)(n+2) + \delta_{m,n+1} m(m+1) \times (m+2)], \quad y\to 0. \quad \text{(A22)}$$

Therefore the polarization function in Eq. (A12) takes the following form:

$$\Pi(\omega,\mathbf{p}) = \frac{2ie^{-y}}{(2\pi l)^2}\sum_{n,m=0}^\infty (-1)^{m+n} \times \int_{-\infty}^\infty \frac{d\omega'}{[\omega'^2 - E_n^2 + i0][(\omega+\omega')^2 - E_m^2 + i0]} \times \{(\omega' + \tilde{\Delta}_0)(\omega+\omega'+\tilde{\Delta}_0)[I_{nm}(y) + I_{n-2,m-2}(y)] + 2\omega_c^2 I_{n-2,m-2}^{(2)}(y)\}. \quad \text{(A23)}$$

After integrating over $\omega'$ in this expression, we obtain

$$\Pi(\omega,\mathbf{p}) = \frac{e^{-y}}{2\pi l^2}\sum_{n,m=0}^\infty \frac{(-1)^{m+n}(E_n+E_m)}{(E_n+E_m)^2-\omega^2}\left[\left(1-\frac{\tilde{\Delta}_0^2}{E_n E_m}\right)[I_{nm}(y) + I_{n-2,m-2}(y)] - \frac{2\omega_c^2}{E_n E_m} I_{n-2,m-2}^{(2)}(y)\right] \quad \text{(A24)}$$

with $I_{nm}, I_{nm}^{(2)} \equiv 0$ for $n<0$ or $m<0$. It is noticeable that the contribution of the LLL (with $n,m=0,1$ and $E_0=E_1=\tilde{\Delta}_0$) in the polarization function is identically zero.

Let us discuss the properties of the static polarization used in the main text in more detail. For the static polarization function $\Pi(\omega=0,\mathbf{p})$ in balanced bilayer graphene, $\tilde{\Delta}_0=0$, we get

$$\Pi(0,\mathbf{p}) = \frac{m}{2\pi\hbar^2} e^{-y}\left\{\sum_{n,m=2}^\infty \frac{(-1)^{n+m}}{M_n M_m (M_n+M_m)} \times \{M_n M_m [I_{n-2,m-2}(y) + I_{nm}(y)] - 2I_{n-2,m-2}^{(2)}(y)\} + 2\sum_{n=2}^\infty \frac{(-1)^n}{M_n}[I_{0n}(y) - I_{1,n}(y)]\right\} \equiv \frac{m}{\hbar^2}\tilde{\Pi}(y), \quad \text{(A25)}$$

where $M_n=\sqrt{n(n-1)}$. Note that the quasiparticle mass $m$ appears as an overall factor only and does not enter the function $\tilde{\Pi}(y)$. We checked that the double sum is convergent and in numerical calculation we took the upper limits in the sum around $n_{\max}, m_{\max}=250$, which is enough to calculate $\tilde{\Pi}(y)$ up to values $y=12$ as it is shown in Fig. 1.

Using Eqs. (A16), (A22), and (A25), we find the asymptotics of the static polarization function at $y\to 0$

$$\tilde{\Pi}(y) \simeq \frac{2y}{\pi}\left[\sum_{n=2}^{\infty}\frac{1}{\sqrt{n}(\sqrt{n+1}+\sqrt{n-1})(n+\sqrt{n^2-1})}+\frac{1}{\sqrt{2}}\right] \approx 0.55y. \tag{A26}$$

The main contribution in this expression (around 80%) comes from the transitions between the LLL and the first higher LL with $n=2$ (the term $1/\sqrt{2}$ in brackets). With increasing $y$, the number of higher LLs providing relevant contributions in the polarization function grows.

In a similar way, one can find the expressions for the two independent polarization functions $\Pi_{11}(0,\mathbf{p})$ and $\Pi_{12}(0,\mathbf{p})$

$$\Pi_{11}(y) = \frac{me^{-y}}{2\pi\hbar^2}\left\{\sum_{n,m=2}^{\infty}\frac{(-1)^{n+m}}{M_nM_m(M_n+M_m)}\{M_nM_m[I_{n-2,m-2}(y) + I_{nm}(y)]\} + 2\sum_{n=2}^{\infty}\frac{(-1)^n}{M_n}[I_{0n}(y)-I_{1,n}(y)]\right\},$$

$$\Pi_{12}(y) = -\frac{me^{-y}}{\pi\hbar^2}\sum_{n,m=2}^{\infty}\frac{(-1)^{n+m}}{M_nM_m(M_n+M_m)}I^{(2)}_{n-2,m-2}(y). \tag{A27}$$

At zero momentum, $y=0$, we have

$$\Pi_{11}(y=0) = -\Pi_{12}(y=0) = \frac{m}{2\pi\hbar^2}\sum_{n=2}^{n_{\max}}\frac{1}{\sqrt{n(n-1)}}. \tag{A28}$$

As is seen, the quantities $\Pi_{11},\Pi_{12}$ are logarithmically divergent separately, and we introduced cutoff $n_{\max}$. The physical origin of this cutoff is the following. For high energy modes, monolayerlike dynamics takes place, whose contribution to $\Pi_{11}(y=0)$ and $\Pi_{12}(y=0)$ is strongly suppressed [recall that in monolayer graphene $\Pi(0)=0$, see for example Ref. 18]. Therefore the cutoff $n_{\max}$ can roughly be estimated from the condition of the applicability of the low-energy effective model:[1] $\hbar\omega_c\sqrt{n(n-1)} < \gamma_1/4$, which gives $n_{\max} \simeq (\gamma_1 l/2\sqrt{2}\hbar v_F)^2 \approx 45/B$ [T] (here the values m, $\gamma_1$, and $v_F$ are taken from Ref. 1).

For the effective dielectric constant $\kappa_{eff}$ in Eq. (A7) we thus get

$$\kappa_{eff} = \kappa + \frac{2me^2d}{\hbar^2}\sum_{n=2}^{n_{\max}}\frac{1}{\sqrt{n(n-1)}} = \kappa + 0.68\sum_{n=2}^{n_{\max}}\frac{1}{\sqrt{n(n-1)}}, \tag{A29}$$

where the value $m \approx 0.054m_e$ was used. With $n_{\max} \approx 45/B$ [T], we find that for the range of fields from 0.25 to 10 T the cutoff $n_{\max}$ varies in the interval 6–180, and therefore the quantity $\kappa_{eff}-\kappa$ varies in the interval 1–4.

*On leave from Bogolyubov Institute for Theoretical Physics, 03680 Kiev, Ukraine.


[1] E. McCann and V. I. Fal'ko, Phys. Rev. Lett. **96**, 086805 (2006).
[2] E. McCann, D. S. L. Abergel, and V. I. Fal'ko, Solid State Commun. **143**, 110 (2007).
[3] K. S. Novoselov, E. McCann, S. V. Morozov, V. I. Fal'ko, M. I. Katsnelson, U. Zeitler, D. Jiang, F. Schedin, and A. K. Geim, Nat. Phys. **2**, 177 (2006).
[4] E. A. Henriksen, Z. Jiang, L.-C. Tung, M. E. Schwartz, M. Takita, Y. J. Wang, P. Kim, and H. L. Stormer, Phys. Rev. Lett. **100**, 087403 (2008).
[5] A. H. Castro Neto, F. Guinea, N. M. R. Peres, K. S. Novoselov, and A. K. Geim, Rev. Mod. Phys. **81**, 109 (2009).
[6] B. E. Feldman, J. Martin, and A. Yacoby, Nat. Phys. **5**, 889 (2009).
[7] Y. Zhao, P. Cadden-Zimansky, Z. Jiang, and P. Kim, Phys. Rev. Lett. **104**, 066801 (2010).
[8] K. Nomura and A. H. MacDonald, Phys. Rev. Lett. **96**, 256602 (2006); K. Yang, S. Das Sarma, and A. H. MacDonald, Phys. Rev. B **74**, 075423 (2006); M. O. Goerbig, R. Moessner, and B. Douçot, *ibid.* **74**, 161407(R) (2006); J. Alicea and M. P. A. Fisher, *ibid.* **74**, 075422 (2006); L. Sheng, D. N. Sheng, F. D. M. Haldane, and L. Balents, Phys. Rev. Lett. **99**, 196802 (2007).
[9] V. P. Gusynin, V. A. Miransky, S. G. Sharapov, and I. A. Shovkovy, Phys. Rev. B **74**, 195429 (2006); I. F. Herbut, Phys. Rev. Lett. **97**, 146401 (2006); Phys. Rev. B **75**, 165411 (2007); J.-N. Fuchs and P. Lederer, Phys. Rev. Lett. **98**, 016803 (2007); M. Ezawa, J. Phys. Soc. Jpn. **76**, 094701 (2007).
[10] Y. Barlas, R. Cote, K. Nomura, and A. H. MacDonald, Phys. Rev. Lett. **101**, 097601 (2008).
[11] K. Shizuya, Phys. Rev. B **79**, 165402 (2009).
[12] M. Nakamura, E. V. Castro, and B. Dora, Phys. Rev. Lett. **103**, 266804 (2009).
[13] R. Nandkishore and L. Levitov, arXiv:0907.5395 (unpublished).
[14] E. V. Gorbar, V. P. Gusynin, and V. A. Miransky, Pis'ma Zh. Eksp. Teor. Fiz. **91**, 334 (2010).
[15] E. V. Gorbar, V. P. Gusynin, and V. A. Miransky, Low Temp. Phys. **34**, 790 (2008); E. V. Gorbar, V. P. Gusynin, V. A. Miransky, and I. A. Shovkovy, Phys. Rev. B **78**, 085437 (2008).
[16] V. P. Gusynin, V. A. Miransky, and I. A. Shovkovy, Phys. Rev. Lett. **73**, 3499 (1994); Phys. Rev. D **52**, 4718 (1995).
[17] D. V. Khveshchenko, Phys. Rev. Lett. **87**, 206401 (2001).
[18] E. V. Gorbar, V. P. Gusynin, V. A. Miransky, and I. A. Shovkovy, Phys. Rev. B **66**, 045108 (2002).
[19] G. Baym and L. P. Kadanoff, Phys. Rev. **124**, 287 (1961); J. M. Cornwall, R. Jackiw, and E. Tomboulis, Phys. Rev. D **10**, 2428 (1974).
[20] F. D. M. Haldane, Phys. Rev. Lett. **61**, 2015 (1988).
[21] N. D. Mermin and H. Wagner, Phys. Rev. Lett. **17**, 1133 (1966).
[22] D. A. Abanin, P. A. Lee, and L. S. Levitov, Phys. Rev. Lett. **96**, 176803 (2006).
[23] J. S. Schwinger, Phys. Rev. **82**, 664 (1951).
[24] One can show that the presence of a maximum in the function $4\pi\tilde{\Pi}(y)$ in Fig. 1 follows from the equality of the polarization charge density $n(r)$ in a magnetic field $B$ and that at $B=0$ as $r \to 0$.
[25] I. S. Gradshteyn and I. M. Ryzhik, *Tables of Integrals, Series, and Products* (Academic Press, New York, 1965).